Fall 2015

A new equivalent dipole-moment source reconstruction method for IC radiated emissions based on near-field scanning

Xiao Ren

Department:

A NEW EQUIVALENT DIPOLE-MOMENT SOURCE RECONSTRUCTION METHOD FOR IC RADIATED EMISSIONS BASED ON NEAR-FIELD SCANNING

by

XIAO REN

A THESIS

Presented to the Faculty of the Graduate School of the

MISSOURI UNIVERSITY OF SCIENCE AND TECHNOLOGY

In Partial Fulfillment of the Requirements for the Degree

MASTER OF SCIENCE IN ELECTRICAL ENGINEERING

2015

Approved by

Dr. Jun Fan, Advisor

Dr. Yaojiang Zhang

Dr. David Pommerenke

ABSTRACT

In this paper, a new dipole-moment model based on near-field scanning for representing equivalent IC radiation emissions on a PCB (Print Circuit Board) is presented. One set of dipoles (both electric dipoles and magnetic dipoles) are used to characterize near-field and far-field radiation from the source. In order to build the model, tangential electric field and magnetic field on a Huygens's box enclosing the radiation source are needed. Both the phase and magnitude of these tangential fields are obtained either in simulation or in measurement by near-field scanning method. Two steps are established to reconstruct the dipole moment. Firstly, a set of dipole array is used to predict far-field radiation from the source with the least-square method. Then, another set of dipoles which make contributions to the near-field only are added in for accurate calculation of near-field. The dipoles used for predicting far-fields are further distributed into dipole arrays but the value summation of them is equal to each of the dipole used for the far-field matching. All types of dipoles used have the same number and are distributed on the area of the same size and positions. Finally, these two sets of dipole together are able to characterize both near-field and far-field radiation from the source simultaneously. Two examples are used to demonstrate the approach. A U-shape trace model is built in HFSS and the dipole-moment model is validated by simulation. In another example, IC radiation is modeled by dipole-moment and the method is verified by measurement data based on near-field scanning technique. This new dipole-moment model can predict both the near-field and far-field radiation well which is useful in analyzing radio-frequency interference issues.

ACKNOWLEDGMENTS

I would like to express my sincere gratitude to Dr. Jun Fan and Dr. Yaojiang Zhang my advisors, for their teaching, instruction, warm encouragement on my research work, financial support to my study and direction for this thesis during my pursuit of the Master's degree.

I would like to thank Dr. David Pommerenke, Dr. James Drewniak, Dr. Daryl Beetner and all other faculties in MST for their teaching in my courses.

I would also like to express my thanks to all the students in the UMR/S&T EMC lab for their team work and help in my research and coursework. It has been my great pleasure to work with you!

Finally, my sincere appreciation goes to my parents for their encouragement, love and unconditional support.

TABLE OF CONTENTS

Page

LIST OF ILLUSTRATIONS

Page

1. INTRODUCTION

1.1. BACKGROUND

As the increasing of digital circuit speed in recent years, electromagnetic compatibility (EMC) problems have been seen as an issue for IC and PCB design [1]. IC is the center of control in electronic systems and plays an important role in supporting progress in the equipment. IC malfunctions due to noise is becoming a more important issue due to these advances. IC noise coupling to RF receiver on PCB is also critical in designing digital/RF systems. Industrial standards and specifications are established to specify the limits of electromagnetic emissions and quantify the immunity performance of ICs. Therefore, significant attentions need to be put in the early design of high speed systems.

Through detailed 3D electromagnetic simulations of ICs and PCBs, the fields surrounding the devices of interest can be analyzed. Further, intra-system near-field coupling can be investigated. However, in practical cases, some circuit manufacturers do not wish to reveal the detailed information of their ICs which makes the IC model to be built in simulations very difficult. Further, it is unrealistic to run full-wave real IC or complex PCB board simulations because it would take excessive simulation memory and time.

This paper presents the dipole-moment model as equivalent radiation source to address the electromagnetic emission from an IC on a PCB. The extracted dipole-moment model based on near-field scanning on Huygens's surface provides a simple method to characterize near-field and far-field radiation. The dipole models, representing the IC

noise source, can be applied in system full-wave simulations to further analyze the coupling to other structures on the PCB.

1.2. MODELING METHODS FOR IC RADIATED EMISSIONS

Many methods are established for developing equivalent models based on near-field scanning for analyzing IC radiated emissions [2]~[7]. In [8], two different approaches are used to obtain the equivalent model, a set of electric dipoles and a set of magnetic dipoles. These methods are carried out with the near-field scanning technique. The fields are obtained on an observation plane above the IC. From [9], the near-field prediction of far-field is studied and the near-field scanning size on the accuracy of far-field estimation is studied. With a large near-field scanning plane, an approximate Huygens'ss surface is assumed. The scanning plane needs to be large enough to get accurate far-field estimation. In real PCB boards, there might be other ICs or structures near the IC of interest so the scanning plane could not be sufficiently large. In this case, approaches using one observation plane become insufficient. In [10], an improved dipole-moment method for predicting near-field and far-field is established. Regularization technique and truncated singular-value decomposition together with the conventional least-square method are investigated for more balanced transfer matrix and thus more accurate dipole-moment model. In this paper, three types of dipoles are used for matching both near-field and far-field. With the presence of the ground plane on PCB and assuming the ground plane is large, image theory is applied. In the far-field, the radiation from some types of dipoles cancel with the radiation from their image dipoles and some add up. The dipole types this paper used are only those dipoles which have contribution to the far-field. However, in the near-field, more evanescent waves are observed and

other types of dipoles that do not contribute to the far-field could also be critical in constructing near-field. Moreover, hundreds of dipoles are used to evaluate near-field and far-field which may result in very large calculation time. When the dipole models are used in system-level simulations, it could also take very long simulation time.

1.3. PROPOSED MODELING METHOD BASED ON NEAR-FIELD SCANNING

This paper presents a method to reconstruct the noise source of a U-shape trace or an actual IC above a large ground plane. The U-shape trace model is built in HFSS. Near-field data is obtained from simulation and the method is verified by simulation results. The near-field tangential E and H fields are obtained by adding 5 observation planes that enclosing the U-shape trace above the ground plane. Then, the E and H field magnitude and phase data is exported from the simulated results. In actual IC measurement, only tangential H fields enclosing the DUT (device under test) are measured. Later on, the H fields on the closed surface is imported to HFSS simulation to further get tangential E fields. And then, the method is verified based on these E and H field data. This method assumes that we don't have detailed information of the IC, only the frequency the IC is working at is known.

In this method, all 6 types of dipoles $\mathbf{J_x}$, $\mathbf{J_y}$, $\mathbf{J_z}$, $\mathbf{M_x}$, $\mathbf{M_y}$ and $\mathbf{M_z}$ are used for representing the equivalent radiation source. These dipoles are located above the U-shape trace or IC. All the dipole locations are very close to the ground plane. $\mathbf{J_x}$, $\mathbf{J_y}$, $\mathbf{M_z}$ dipole together with their image will have no radiation in the far field but they contribute to the near-field. $\mathbf{J_z}$, $\mathbf{M_x}$ and $\mathbf{M_y}$ dipoles only contribute to the far-field. When building the dipole-moment model, far-field and near-field are matched with dipoles separately. Firstly, far-field are calculated based on Huygens's Principle with known tangential E

and H field on a closed surface and matched by $\mathbf{J_z}$, $\mathbf{M_x}$ and $\mathbf{M_y}$ dipoles. Then, another set of dipoles $\mathbf{J_x}$, $\mathbf{J_y}$ and $\mathbf{M_z}$ are added to the calculated $\mathbf{J_z}$, $\mathbf{M_x}$ and $\mathbf{M_y}$ in the previous step to match the near-field on the same Huygens's surface. $\mathbf{J_z}$, $\mathbf{M_x}$ and $\mathbf{M_y}$ dipoles that used for matching the far-field are further divided into dipole arrays for matching near-field together with $\mathbf{J_x}$, $\mathbf{J_y}$ and $\mathbf{M_z}$ dipoles. The value summation of the $\mathbf{J_z}$, $\mathbf{M_x}$ and $\mathbf{M_y}$ dipole arrays will be equal to the original values obtained from the far-field fitting process. The array sizes for all six types of dipoles are the same, and distributed on the area size of the IC. All these 6 types of dipoles together will give good prediction of both near-field and far-field.

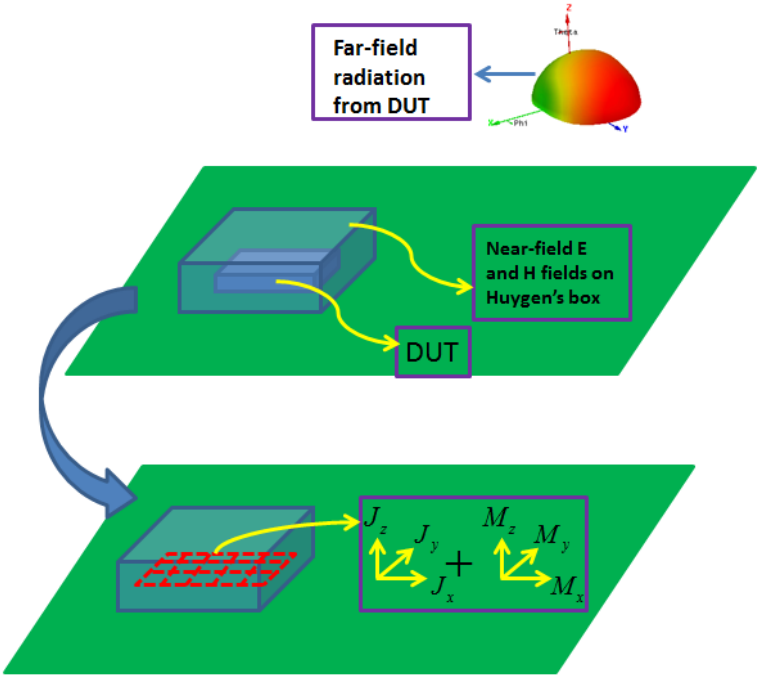

Figure 1.1 Equivalent sources representing near- and far-field radiation from DUT

All types of dipoles are located uniformly on a rectangular area about the size of the DUT. The magnitude and phase of the dipoles are calculated with the least-square method. The normalization from [10] is adopted in the least-square algorithm to have a more balanced transfer matrix and thus more accurate result. The dipoles numbers are chosen to have an optimized condition number of the transfer matrix which will result in relative small least-square error.

The method proposed in this paper is verified by two examples, simulated U-shape trace and measured actual IC. The dipole model can have a good prediction of field outside of the Huygens's surface for both near-field and far-field. Also, the dipole model is capable of predicting field coupling and induced voltage when applied in system-level simulations. The accuracy of matching near-field and far-field is significantly increased compared with methods in [8]. Matching near-field and far-field separately with all 6 types of dipoles takes account of the dipoles that contribute to the evanescent waves in the near-field. With a better understanding of radiation physics in the near-field and far-field, the dipole number in the proposed method is significantly reduced compared with method in [10].

2. NEAR-FIELD SCANNING METHOD

2.1. HUYGENS'Ss PRINCIPLE

Huygens's principle is a more rigorous formulation of field equivalence. The equivalence principle is based on the uniqueness theorem. It demonstrates that if the tangential electric and magnetic fields are completely known over a closed surface, the fields in the source-free region can be determined [11].

The fields outside of an imaginary closed surface can be obtained if suitable electric- and magnetic-current densities are placed over this surface that satisfies the boundary conditions. The formulation is exact but the accuracy is depending on the information of the tangential electric and magnetic fields known over the closed surface. The current density is integrated over small "segments" which define a current distribution on it. In Figure 2.1 , the original source inside of the closed surface is removed. Assuming the fields E and H are inside S, E1 and H1 are outside of S. These fields must satisfy the boundary conditions on the tangential electric and magnetic field components.

$$\mathbf{J}_s = \hat{\mathrm{n}} \times [\mathbf{H}_1 - \mathbf{H}] \tag{1}$$

$$\mathbf{M}_s = -\hat{\mathrm{n}} \times [\mathbf{E}_1 - \mathbf{E}] \tag{2}$$

Because the fields E and H within S are not the region of interest, they can be assumed zero. In this case, the equivalent problem can be written as:

$$\mathbf{J}_s = \hat{\mathrm{n}} \times [\mathbf{H}_1 - \mathbf{H}]\big|_{\mathbf{H}=0} = \hat{\mathrm{n}} \times \mathbf{H}_1 \tag{3}$$

$$\mathbf{M}_s = \hat{\mathrm{n}} \times [\mathbf{E}_1 - \mathbf{E}]\big|_{\mathbf{E}=0} = \hat{\mathrm{n}} \times \mathbf{E}_1 \tag{4}$$

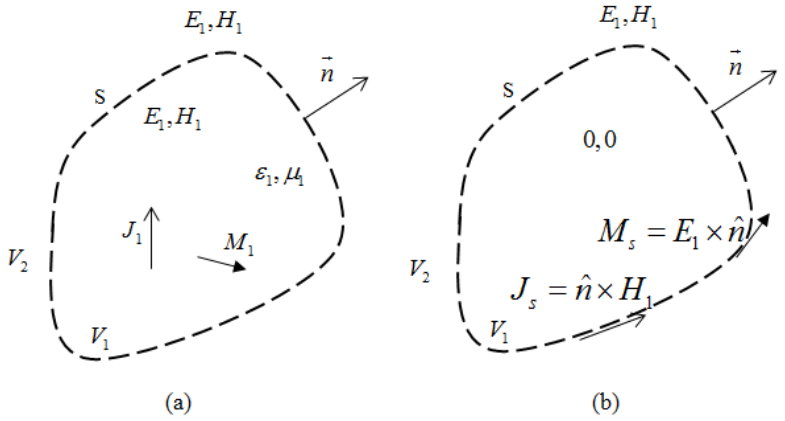

Figure 2.1 (a) actural problem (b) equivalent problem

With near-field scanning technique, the tangential E and H fields on the closed surface enclosing the DUT can be obtained. In the U-shape trace radiation simulation, the tangential E and H fields are obtained on 5 surfaces. Image theory is further applied in calculating near-field and far-field with the Huygens's principle. In the case of measuring near-field of the IC on a closed surface, only H field on the top surface and 4 tangential H field lines on the side walls as shown in Figure.2.2. Here it is assumed that the scanning box is very close to the ground and the H fields on the 4 side walls are constant values. The tangential H field on 5 surfaces enclosing the IC is imported into HFSS simulation to obtain tangential E fields. In HFSS simulation, an infinitely large ground plane is added

to the bottom surface to be consistent with measurement setup. Inside of the measurement box is set as PML boundary.

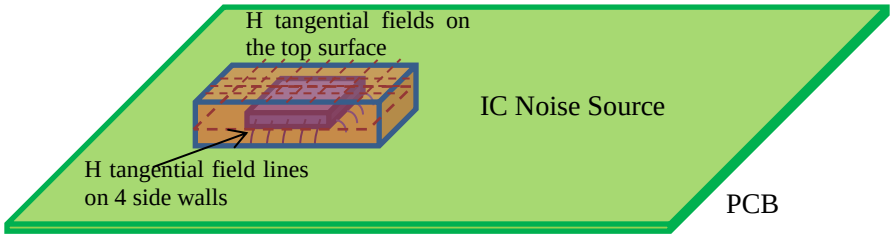

Figure 2.2 IC near-field scanning

2.2. NEAR-FIELD MEASUREMENT METHODOLOGY

The near-field magnitude and phase of tangential E and H are measured by a scanning field probe over a preselected surface. The surface could be a plane, a cylinder or a sphere. The planar scanning method is suitable for high gain antennas and requires the least measurement effort. However, in real IC radiation near-field measurement, the radiation pattern tends to be omnidirectional and the scanning plane needs to be large. In this paper, tangential H fields of the IC on a cuboid are measured.

An IC array above a large ground plane is shown in Figure 2.3. Measurement of H tangential near-field on a closed box is used to validate the dipole-moment model. H field probe is used here to measure the radiation from the IC at 125MHz.

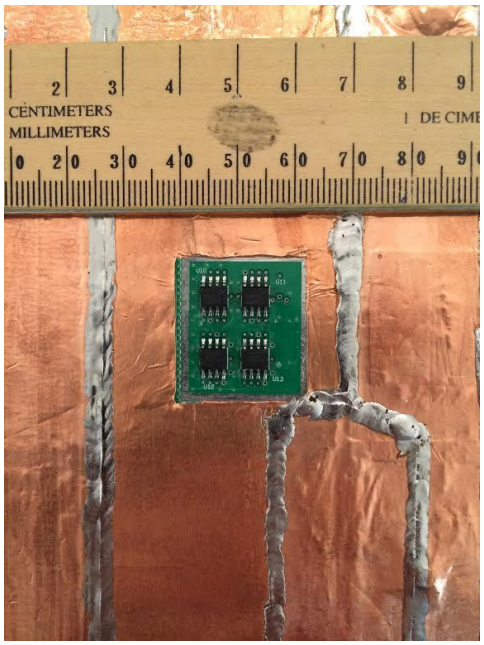

Figure 2.3 IC array above a large ground plane

3. DEVELOPMENT OF THE EQUIVALENT DIPOLE MODEL

3.1. EQUIVALENT DIPOLE MODEL BASICS

This method is aiming at replacing emission from an IC above a large ground plane with an array of equivalent dipoles that will generate the same fields with those from the IC. The emission from the IC is normally from the current inside of it. There are total 6 types of infinitesimal dipoles $\mathbf{J_x}$, $\mathbf{J_y}$, $\mathbf{J_z}$, $\mathbf{M_x}$, $\mathbf{M_y}$ and $\mathbf{M_z}$ that could be used as equivalent sources to represent the emission from an elemental current. In general, no information of the detailed IC is required except for the dimension and the operation frequency. The dipole array is normally placed on the size of the IC area. Considering the fact that most IC is relatively thin, the dipole locations are in a planar surface 1~2mm above the IC.

3.2. RADIATION FROM DIPOLES

This method is aiming at replacing emission from an IC above a large ground plane with an array of equivalent dipoles that will generate the same fields with those from the IC.

3.2.1. Dipole Radiation in Free Space. There are two steps needed to find the fields radiated by the current element. The first step is to determine A and then find E and H. Assume a dipole locates at (x', y', z') with an orientation of $\mathbf{a} = (a_x, a_y, a_z)$. Its current and length are I and l, respectively. The vector potential is $\mathbf{A} = \mu IlG(\mathbf{r}, \mathbf{r}')\mathbf{a}$ where $G(\mathbf{r}, \mathbf{r}') = e^{-jkR} / 4\pi R$ and $R = \sqrt{(x - x')^2 + (y - y')^2 + (z - z')^2}$. Here, (x, y, z) represent the observation point coordinates, (x', y', z') represent the coordinates of the source. R is the distance from any point on the source to the observation point.

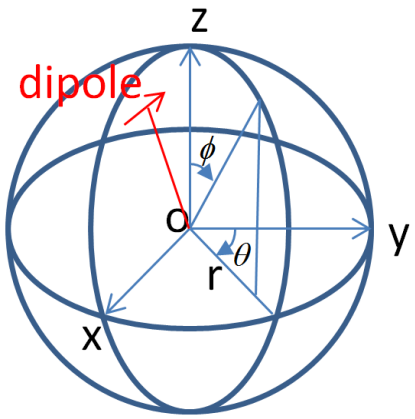

Figure 3.1 Dipole radiation in spherical coordinates system

Radiated fields from electric current J can be expressed as:

$$\mathbf{E}^{J}(\mathbf{r}) = jk\eta\int_{V}\begin{Bmatrix} 2\left[(jkR)^{-1}+(jkR)^{-2}\right]\left[\mathbf{J}(\mathbf{r}')\cdot\hat{\mathbf{R}}\right]\hat{\mathbf{R}} \\ -\left[1+(jkR)^{-1}+(jkR)^{-2}\right]\left[\mathbf{J}(\mathbf{r}')-(\mathbf{J}(\mathbf{r}')\cdot\hat{\mathbf{R}})\hat{\mathbf{R}}\right] \end{Bmatrix} G(R)dV \tag{7}$$

$$\mathbf{H}^{J}(\mathbf{r}) = jk\int_{V}\left[\left(1+(jkR)^{-1}\right)\mathbf{J}(\mathbf{r}')\times\hat{\mathbf{R}}\right]G(R)dV \tag{8}$$

Radiated fields by magnetic current M can be expressed as:

$$\mathbf{E}^{M}(\mathbf{r}) = -jk\int_{V}\left[\left(1+(jkR)^{-1}\right)\mathbf{M}(\mathbf{r}')\times\hat{\mathbf{R}}\right]G(R)dV \tag{9}$$

$$\mathbf{H}^{M}(\mathbf{r}) = jk/\eta\int_{V}\begin{Bmatrix} 2\left[(jkR)^{-1}+(jkR)^{-2}\right]\left[\mathbf{M}(\mathbf{r}')\cdot\hat{\mathbf{R}}\right]\hat{\mathbf{R}} \\ -\left[1+(jkR)^{-1}+(jkR)^{-2}\right]\left[\mathbf{M}(\mathbf{r}')-(\mathbf{M}(\mathbf{r}')\cdot\hat{\mathbf{R}})\hat{\mathbf{R}}\right] \end{Bmatrix} G(R)dV \tag{10}$$

Dipoles are point sources and vector sources. Dipoles are one kind of source that has their dipole moments, orientations and locations.

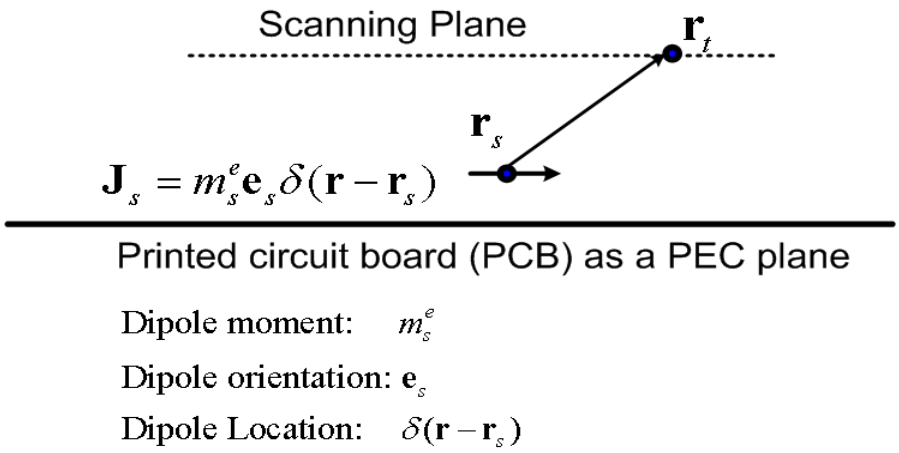

Figure 3.2 Electric dipole source

Radiation from electric and magnetic dipole moment can be further written as:

$$\mathbf{E}^J(\mathbf{r}_t) = \sum_{s=1}^{N_e^J} m_s^J \, jk \begin{Bmatrix} [1+3(jkR_{ts})^{-1}+3(jkR_{ts})^{-2}][\mathbf{e}_s^J \cdot \hat{\mathbf{R}}_{ts}]\hat{\mathbf{R}}_{ts} \\ -[1+(jkR_{ts})^{-1}+(jkR_{ts})^{-2}]\mathbf{e}_s^J \end{Bmatrix} G(R_{ts}) \tag{11}$$

$$\eta \mathbf{H}^J(\mathbf{r}_t) = \sum_{s=1}^{N_e^J} m_s^J \, jk \left[\left(1+\frac{1}{jkR_{ts}} \right) \mathbf{e}_s^J \times \hat{\mathbf{R}}_{ts} \right] G(R_{ts}) \tag{12}$$

$$\mathbf{E}^M(\mathbf{r}_t) = \sum_{s=1}^{N_e^M} m_s^M \left[-jk \left(1+\frac{1}{jkR_{ts}} \right) \mathbf{e}_s^M \times \hat{\mathbf{R}}_{ts} \right] G(R_{ts}) \tag{13}$$

$$\eta \mathbf{H}^J(\mathbf{r}_t) = \sum_{s=1}^{N_e^M} m_s^M \, jk \begin{Bmatrix} [1+3(jkR_{ts})^{-1}+3(jkR_{ts})^{-2}][\mathbf{e}_s^M \cdot \hat{\mathbf{R}}_{ts}]\hat{\mathbf{R}}_{ts} \\ -[1+(jkR_{ts})^{-1}+(jkR_{ts})^{-2}]\mathbf{e}_s^M \end{Bmatrix} G(R_{ts}) \tag{14}$$

Where $\mathbf{J}(\mathbf{r}') = \sum_{s=1}^{N_e^J} m_s^J \mathbf{e}_s^J \delta(\mathbf{r}' - \mathbf{r}_s^J)$, and $\mathbf{M}(\mathbf{r}') = \sum_{s=1}^{N_e^M} m_s^M \mathbf{e}_s^M \delta(\mathbf{r}' - \mathbf{r}_s^M)$

3.2.2. Image Theory. In the case under study, the IC is located above a very large ground plane. The image theory is applied to calculate the radiation from dipoles with the presence of the ground plane. Image theory removes the ground plane and places a virtual image source on the other side of the ground plane. Image theory will give the correct fields to the right of the conducting plane.

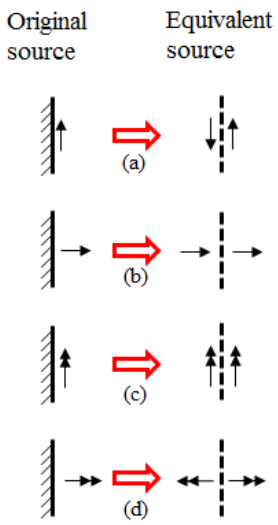

Figure 3.3 Electric and magnetic current images. (a) An electric current parallel to a ground plane. (b) An electric current normal to a ground plane. (c) A magnetic current parallel to a ground plane. (d) A magnetic current normal to a ground plane

An electric current parallel to a ground plane will have its image current in the opposite direction. The image of an electric current normal to a ground plane will be in the same direction with the original current. A magnetic current parallel to a ground plane will have its image current in the same direction with the original current. If the magnetic

current is normal to the ground plane, its image will be in the opposite direction with the original source. The near-field and far-field emission from the IC could be represented by the radiation from the equivalent sources and their images.

3.2.3. Equivalent Dipole Reconstruction Method. All 6 types of dipoles $\mathbf{J_x}$, $\mathbf{J_y}$, $\mathbf{J_z}$, $\mathbf{M_x}$, $\mathbf{M_y}$, $\mathbf{M_z}$ are used to represent the IC noise source. This set of dipoles should radiate the same near- and far-field as the real IC above a large ground plane. The dipole values (both magnitude and phase) could be determined by fitting the near-field and far-field to find a solution of the inverse problem. First, the tangential E and H fields on a closed surface enclosing the DUT are obtained either in simulation or measurement. Then, the far-field radiation from the DUT is calculated based on the Huygens's Principle with the known tangential E and H fields on the 5 surfaces. $\mathbf{J_z}$, $\mathbf{M_x}$ and $\mathbf{M_y}$ dipole are chosen to match the far-field radiation. In the far-field, r is large and since $\mathbf{J_x}$, $\mathbf{J_y}$ and $\mathbf{M_z}$ dipole's radiation cancel with the radiation from their image, they make nearly no contribution to the far-field.

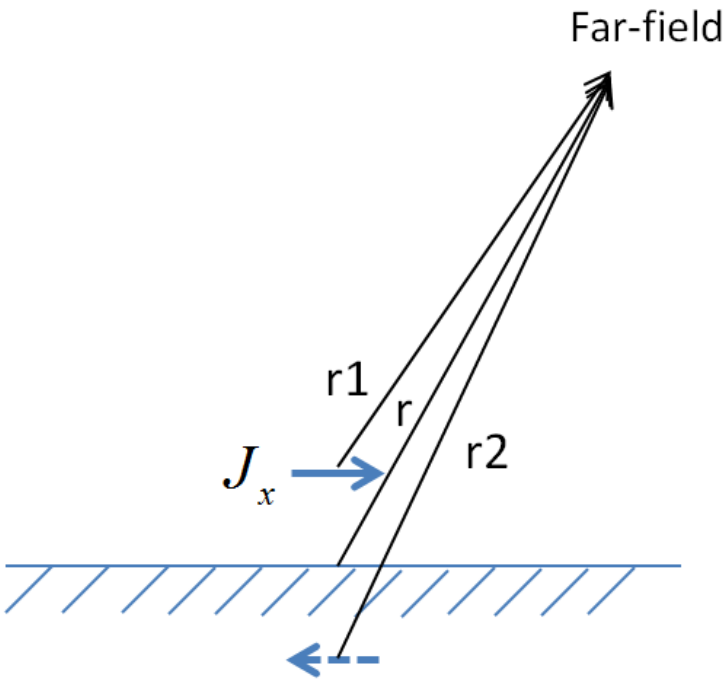

Figure 3.4 $\mathbf{J_x}$ dipole and its image radiation in the far-field

The $\mathbf{J_z}$, $\mathbf{M_x}$ and $\mathbf{M_y}$ dipoles are placed uniformly on a rectangle area at the center of the DUT 1mm above it. With known $\mathbf{J_z}$, $\mathbf{M_x}$ and $\mathbf{M_y}$ dipole location, these dipoles and their radiated fields are related by expression (11). $\mathbf{m^J}$ and $\mathbf{m^M}$ are dipole moments.

$$\begin{bmatrix} [\mathbf{E}_\theta]_{M^2\times 1} \\ [\mathbf{E}_\phi]_{M^2\times 1} \\ [\mathbf{H}_\theta]_{M^2\times 1} \\ [\mathbf{H}_\phi]_{M^2\times 1} \end{bmatrix} = \mathbf{T}_1 \begin{bmatrix} [\mathbf{m}^{J_z}]_{N^2\times 1} \\ [\mathbf{m}^{M_x}]_{N^2\times 1} \\ [\mathbf{m}^{M_y}]_{N^2\times 1} \end{bmatrix} \tag{15}$$

E_θ, E_ϕ, H_θ and H_ϕ are the θ and ϕ-directional components of the electric and magnetic fields in the far-field. The number of observation points in the far-field is M*M. $\mathbf{J_z}$, $\mathbf{M_x}$ and $\mathbf{M_y}$ are electric and magnetic dipole that are distributed as an array above the

IC. The number of each type of dipole is N*N. T is the transfer matrix relates the dipole value and their radiated fields and can be expressed as:

$$\mathbf{T}_1 = \begin{pmatrix} T_{E_\theta J_z} & T_{E_\theta M_x} & T_{E_\theta M_y} \\ T_{E_\phi J_z} & T_{E_\phi M_x} & T_{E_\phi M_y} \\ T_{H_\theta J_z} & T_{H_\theta M_x} & T_{H_\theta M_y} \\ T_{H_\phi J_z} & T_{H_\phi M_x} & T_{H_\phi M_y} \end{pmatrix} \tag{16}$$

The transfer matrix T can be obtained assuming the $\mathbf{J_z}$, $\mathbf{M_x}$ and $\mathbf{M_y}$ dipole moments are 1, and calculate the radiated far-field with equations (7)~(10). The calculated radiated field matrix will be equal to the transfer matrix. The transfer matrix T can be divided into 12 parts. For example $T_{E_\theta J_z}$ represents the relationship between $\mathbf{J_z}$ dipoles and their contribution to the far-field E_θ component. After obtaining the transfer matrix, the equation (11) needs to be solved to find the equivalent dipoles which is a typical inverse problem.

The fields data and the transfer matrix firstly need to be normalized first to have a more accurate solution to the inverse problem. In the far-field, the E and H fields have a magnitude difference of 377 which is the wave impedance. With normalization, E and H fields will be on the same magnitude level. The field matrix is normalized as:

$$\mathbf{F}_n = \begin{bmatrix} [\mathbf{E}_\theta]_{M^2\times 1} / \mathbf{E}_{\theta\max} \\ [\mathbf{E}_\phi]_{M^2\times 1} / \mathbf{E}_{\phi\max} \\ [\mathbf{H}_\theta]_{M^2\times 1} / \mathbf{H}_{\theta\max} \\ [\mathbf{H}_\phi]_{M^2\times 1} / \mathbf{H}_{\phi\max} \end{bmatrix} \tag{17}$$

where $E_{\theta max}$, $E_{\phi max}$, $H_{\theta max}$, $H_{\phi max}$ represent the maximum value of the E_θ, E_ϕ, H_θ and H_ϕ value matrix. The transfer matrix can also be normalized accordingly:

$$\mathbf{T}_n = \begin{pmatrix} T_{E_\theta J_z}/E_{\theta\max} & T_{E_\theta M_x}/E_{\theta\max} & T_{E_\theta M_y}/E_{\theta\max} \\ T_{E_\phi J_z}/E_{\phi\max} & T_{E_\phi M_x}/E_{\phi\max} & T_{E_\phi M_y}/E_{\phi\max} \\ T_{H_\theta J_z}/H_{\theta\max} & T_{H_\theta M_x}/H_{\theta\max} & T_{H_\theta M_y}/H_{\theta\max} \\ T_{H_\phi J_z}/H_{\phi\max} & T_{H_\phi M_x}/H_{\phi\max} & T_{H_\phi M_y}/H_{\phi\max} \end{pmatrix} \tag{18}$$

The dipole value matrix $\mathbf{X_k}$ can be calculated based on the least-square method and the solution can be expressed as:

$$\mathbf{X}_k = [\mathbf{T}_{nk}{}'\mathbf{T}_{nk}]^{-1}\mathbf{T}_{nk}{}'\mathbf{F}_n \tag{19}$$

After solving the inverse problem, a set of dipoles $\mathbf{J_z}$, $\mathbf{M_x}$ and $\mathbf{M_y}$ are calculated for matching the far-field.

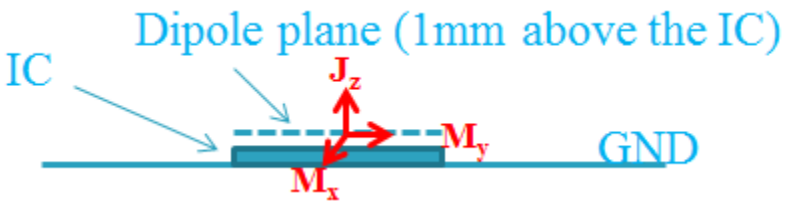

Figure 3.5 $\mathbf{J_z}$, $\mathbf{M_x}$ and $\mathbf{M_y}$ dipoles are chose to predict far-field

The next step is to use a set of dipoles to match the near-field. As discussed earlier, $\mathbf{J_x}$, $\mathbf{J_y}$ and $\mathbf{M_z}$ dipoles make no contribution to the far-field but to the near-field. $\mathbf{J_x}$, $\mathbf{J_y}$ and $\mathbf{M_z}$ dipoles are added to the $\mathbf{J_z}$, $\mathbf{M_x}$ and $\mathbf{M_y}$ dipoles solved in the last step to have a good match of near-field. As the near-field data is on a closed surface enclosing the DUT, Ex, Ey, Ez, Hx, Hy and Hz corresponds to the tangential fields on all five surfaces. In the dipole value matrix, some modifications are made to the $\mathbf{J_z}$, $\mathbf{M_x}$ and $\mathbf{M_y}$ dipoles solved for matching the far-field. When the observation points are far from the source, only a few dipoles are needed to match far-field. But when the observation points are close to the source, the $\mathbf{J_z}$, $\mathbf{M_x}$ and $\mathbf{M_y}$ dipoles need to be divided into multiple dipoles to match the near-field pattern better. For example, $\mathbf{J_z}$ is now divided into a dipole array on a rectangular area. The dipole value summation of all the divided $\mathbf{J_z}$ dipoles needs to be the same with the original $\mathbf{J_z}$ dipole value. $\mathbf{J_x}$, $\mathbf{J_y}$ and $\mathbf{M_z}$ dipoles are also dipole arrays on a rectangular area. The additional constraints are: $\mathbf{m^{Jz} = m^{Jz1} + m^{Jz2} +\dots m^{Jz16}}$, $\mathbf{m^{Mx} = m^{Mx1} + m^{Mx2} +\dots m^{Mx16}}$, and $\mathbf{m^{My} = m^{My1} + m^{My2} +\dots m^{My16}}$

$$\begin{bmatrix} [\mathbf{E}_x]_{P_1^2\times 1} \\ [\mathbf{E}_y]_{P_1^2\times 1} \\ [\mathbf{E}_z]_{P_2^2\times 1} \\ [\mathbf{H}_x]_{P_1^2\times 1} \\ [\mathbf{H}_y]_{P_1^2\times 1} \\ [\mathbf{H}_z]_{P_2^2\times 1} \end{bmatrix} = \mathbf{T}_2 \begin{bmatrix} [\mathbf{m}^{J_x}]_{Q_1^2\times 1} \\ [\mathbf{m}^{J_y}]_{Q_1^2\times 1} \\ [\mathbf{m}^{J_z}]_{Q_2^2\times 1} \\ [\mathbf{m}^{M_x}]_{Q_2^2\times 1} \\ [\mathbf{m}^{M_y}]_{Q_2^2\times 1} \\ [\mathbf{m}^{M_z}]_{Q_1^2\times 1} \end{bmatrix} \tag{20}$$

For example, $\mathbf{J_z}$, $\mathbf{M_x}$ and $\mathbf{M_y}$ dipole each is separated into 16 dipoles. Equation (16) needs to be modified accordingly with the additional constraints.

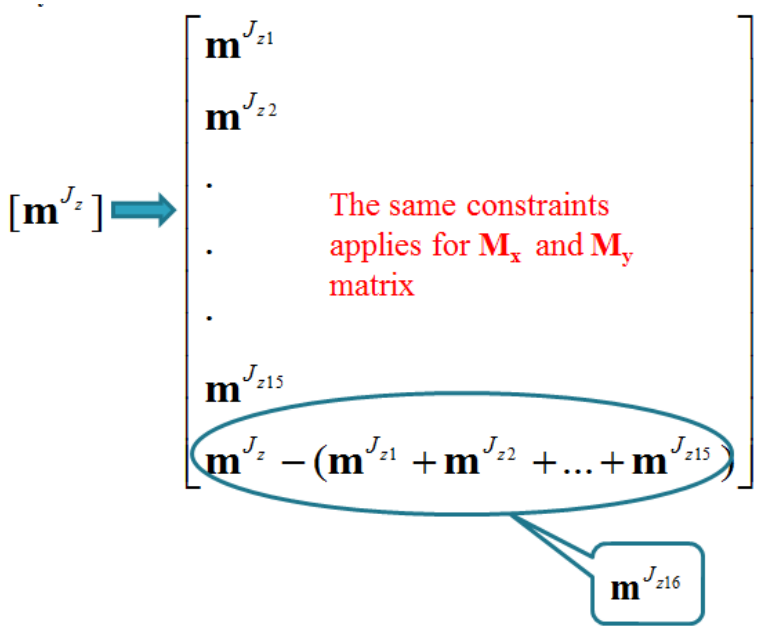

Figure 3.6 Additional constraints for $\mathbf{J_z}$, $\mathbf{M_x}$ and $\mathbf{M_y}$ dipoles

With additional constraints added for the dipole-moment matrix, the number of unknowns to be solved is reduced by one. The solution to the equation can be simply explained by looking at a 2 by 2 transfer matrix with 2 unknowns y_1 and y_2 to be solved. The additional constraint is $y=y_{1+} y_2$.

$$\begin{bmatrix} x_1 \\ x_2 \end{bmatrix} = \begin{bmatrix} a & b \\ c & d \end{bmatrix} \begin{bmatrix} y_1 \\ y_2 \end{bmatrix} = \begin{bmatrix} a & b \\ c & d \end{bmatrix} \begin{bmatrix} y_1 \\ y - y_1 \end{bmatrix} \tag{21}$$

Then y_1 will be the only unknown to be solved. $y_1 = (x_1 - by)/(a-b)$ The same modification of the equation applies for matrix with any dimension.

After solving the equation, a complete set of dipoles of $\mathbf{J_x}$, $\mathbf{J_y}$, $\mathbf{J_z}$, $\mathbf{M_x}$, $\mathbf{M_y}$ and $\mathbf{M_z}$ are obtained to have a good representation of near-field and far-field radiation from the source. The solved equivalent dipoles can be verified by calculating the fields on an arbitrary height by the dipoles and compare them with simulation or measurement results.

3.2.4. U-shape Trace Simulation Validation. A U-shape trace above a large ground plane simulation model is built in commercial software HFSS to validate the dipole reconstruction algorithm. The total length of the U-shape trace is 3cm with each side 1cm. One end of the U-shape trace is excited with 1V voltage source and the other end is terminated with 50Ohm. The ground plane in the simulation model is set as infinite large. Radiation boundary condition is enforced in the simulation setup and the air box size is 100mm*100mm*100mm.

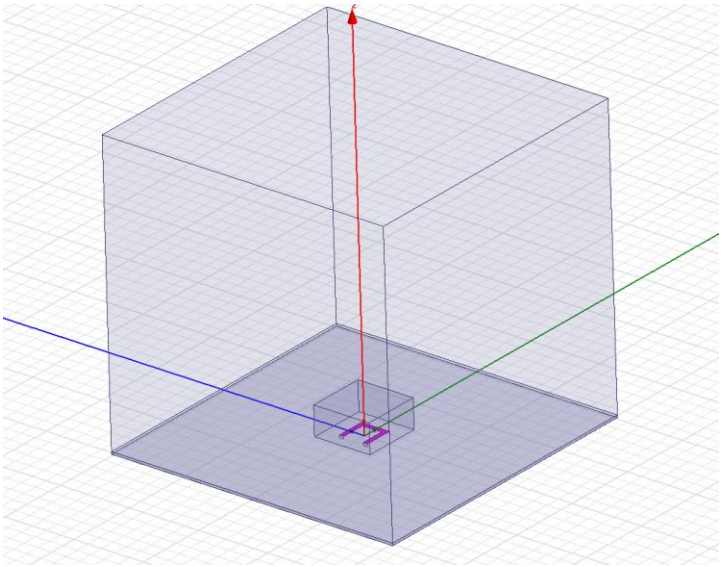

Figure 3.7 U-shape HFSS simulation setup

The dielectric between the ground plane and the trace is FR4_epoxy with Eps_r is 4.4 and loss tangent 0.02. The simulation model is solved at 1GHz.

Tangential E and H fields are obtained on five surfaces (Huygens'ss surface) enclosing the DUT. The observation cuboid size is 20mm*20mm*10mm. The tangential E and H fields magnitudes can be plot in HFSS and the fields data can be exported for further calculaton.

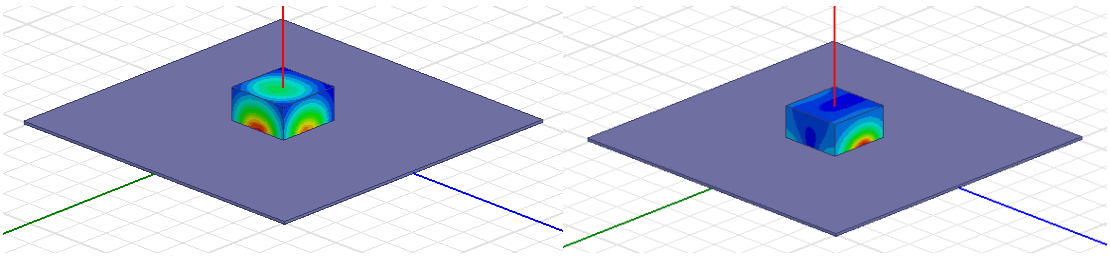

(a) (b)

Figure 3.8 (a) Tangential E field on the Huygens'ss box (b) Tangential H field on the Huygens'ss box

First, far-field $\mathbf{E}_\theta$, $\mathbf{E}_\phi$, $\mathbf{H}_\phi$ and $\mathbf{H}_\theta$ are calculated based on Huygens'ss Principle. Then, $\mathbf{J_z}$, $\mathbf{M_x}$ and $\mathbf{M_y}$ dipoles are used to match the far-field by solving the inverse problem. Only one dipole of each type could have a good match of far-field. The three types of dipole are all placed at the center of the U-shape trace 1mm above it. When

solving the inverse problem, the condition number of the transfer matrix need to be carefully taken into account to have a more accurate solution of the dipole values.

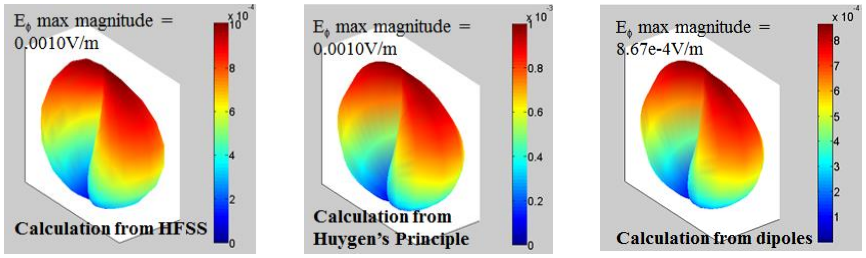

(a) (b) (c)

Figure 3.9 Far-field $\mathbf{E}_\phi$ comparison on 3m sphere between (a) HFSS simulation (b) Huygens'ss calculation (c) Equivalent dipole calculation

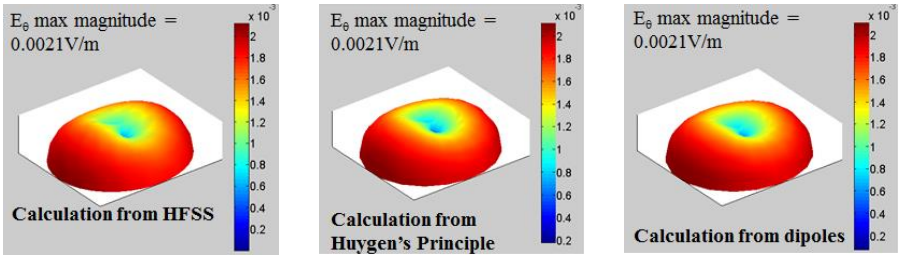

(a) (b) (c)

Figure 3.10 Far-field $\mathbf{E}_\theta$ comparison on 3m sphere between (a) HFSS simulation (b) Huygens's calculation (c) Equivalent dipole calculation

The far-field radiation on 3m sphere from both Huygens's calculation and dipole calculation is compared. The far-field $\mathbf{E}_\theta$ and $\mathbf{E}_\phi$ patterns from Huygens'ss calculation and from dipole reconstruction agree well. The maximum values also match well.

Then, $\mathbf{J_z}$, $\mathbf{M_x}$, and $\mathbf{M_y}$ dipole each is divided into 4 dipoles. The dipole is uniformally distributed as an array located 1mm above the U-shape trace on a rectangle with area size of 4mm*4mm in the middle of the DUT. $\mathbf{J_x}$, $\mathbf{J_y}$ and $\mathbf{M_z}$ dipoles are added to the dipoles which are distributed on the same area with the same number.

The tangential E and H fields on the top surface from Huygens's calculation is shown in the following figure.

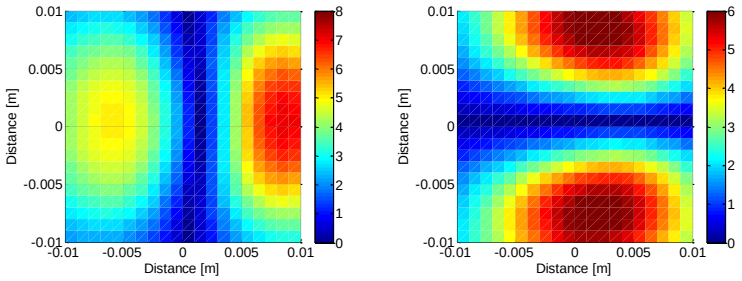

(a) (b)

Figure 3.11 Tangential E fields magnitude on top surface of the Huygens's box from simulation (a) E_x (b) E_y

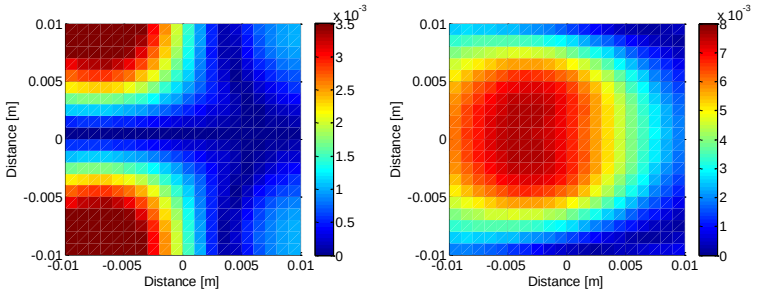

(a) (b)

Figure 3.12 Tangential H fields magnitude on top surface of the Huygens's box from simulation (a) H_x (b) H_y

The tangential fields calculated from all 6 types of dipoles together is shown in the following figure.

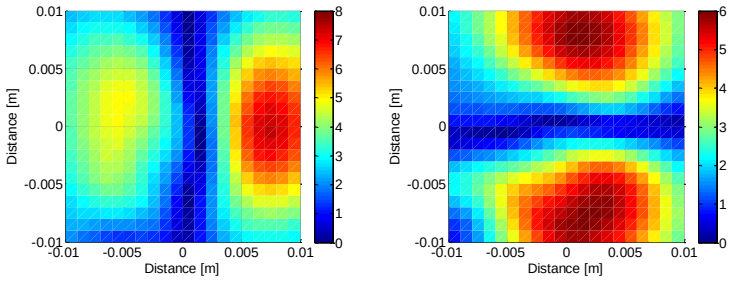

(a) (b)

Figure 3.13 Tangential E fields magnitude on top surface of the Huygens's box from dipole reconstruction (a) E_x (b) E_y

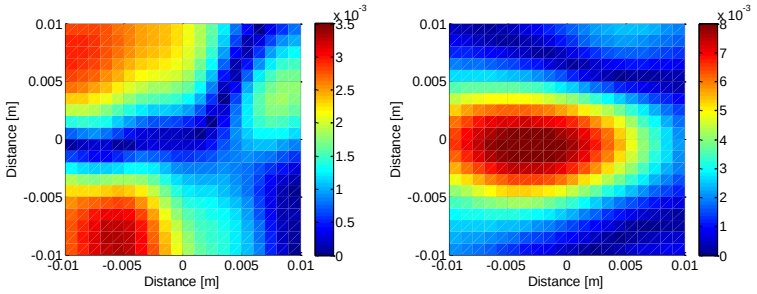

(a) (b)

Figure 3.14 Tangential H fields magnitude on top surface of the Huygens's box from dipole reconstruction (a) H_x (b) H_y

If only $\mathbf{J_z}$, $\mathbf{M_x}$, and $\mathbf{M_y}$ dipoles are used, which is the conventional method for matching the near-field on the Huygens'ss surface, also with the distribution of the three types of dipoles into an array, the magnitude of the consturcted fields will have a big difference. This shows the other three types of dipoles are needed to add in for more accurate of near-field prediction.

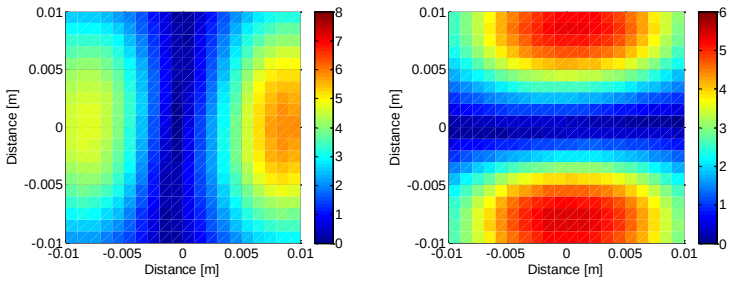

(a) (b)

Figure 3.15 Tangential E fields magnitude on top surface of the Huygens's box from dipole reconstruction (only $\mathbf{J_z}$, $\mathbf{M_x}$, and $\mathbf{M_y}$ dipoles are used) (a) E_x (b) E_y

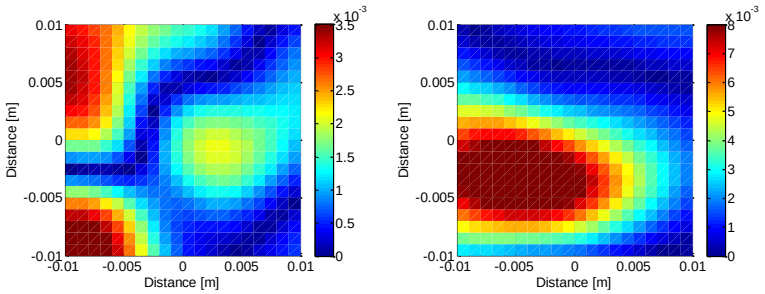

(a) (b)

Figure 3.16 Tangential H fields magnitude on top surface of the Huygens's box from dipole reconstruction (only $\mathbf{J_z}$, $\mathbf{M_x}$, and $\mathbf{M_y}$ dipoles are used) (a) H_x (b) H_y

The E and H tangential fields on the top surface from Huygens's calculation and dipole reconstruction match well in both patterns and magnitudes. The dipole model is further validated by calculating the fields on a large observation plane at 20mm height.

The tangential E and H fields from equivalent dipole calculation showed resonable agreement with the HFSS simulation results.

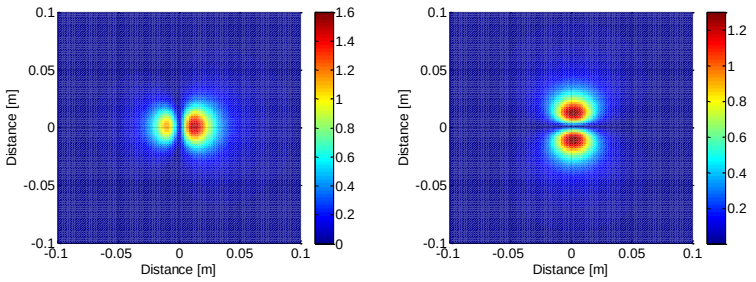

(a) (b)

Figure 3.17 Tangential E fields magnitude on 20mm height from equivalent dipole calculation (a) E_x (b) E_y

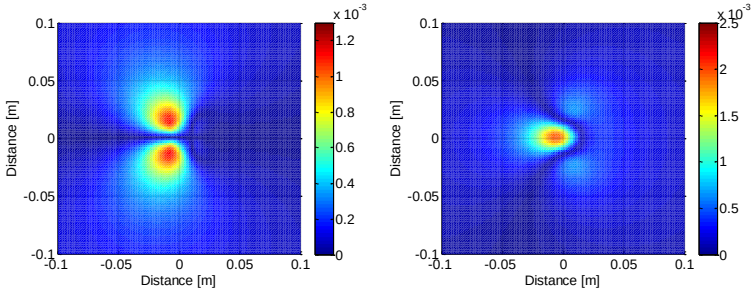

(a) (b)

Figure 3.18 Tangential H fields magnitude on 20mm height from equivalent dipole calculation (a) H_x (b) H_y

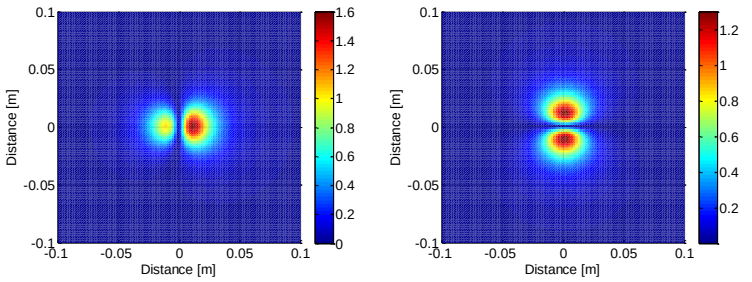

(a) (b)

Figure 3.19 Tangential E fields magnitude on 20mm height from Huygens's Principle calculation (a) E_x (b) E_y

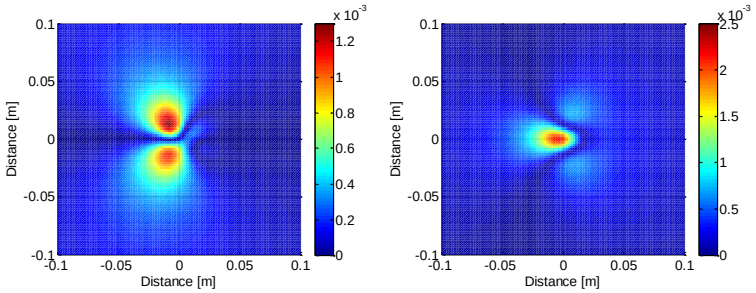

(a) (b)

Figure 3.20 Tangential H fields magnitude on 20mm height from Huygens's Principle calculation (a) H_x (b) H_y

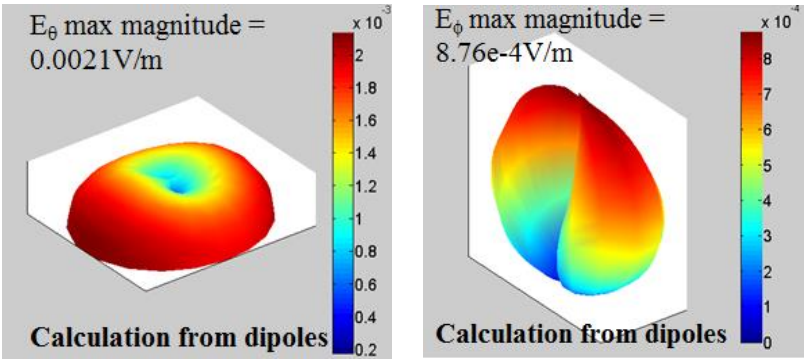

Figure 3.21 Far-field magnitude at 3m calculation from all 6 types of dipoles

The far-field is further calculated by the extracted 6 types of dipoles. The calculated results are compared with the results from Huygens's Principle and they match well in radiation pattern and magnitude. $\mathbf{J_x}$, $\mathbf{J_y}$ and $\mathbf{M_z}$ dipoles have negligible effect on the far-field magnitude. It validates that the equivalent dipole model is able to predict both near- and far-field well simultaneously.

3.2.5. IC Radiation Measurement Validation. The algorithm is validated based on real IC radiation measurement. The IC operates at 125MHz, 1GHz and 2GHz. Only tangential H fields are obtained from near-field scanning on the Huygens's surface. Since the IC is very close to the ground plane, H field on the top surface and 4 lines on the side walls are measured. The scanning area is a cuboid with size 50mm*60mm*5mm. The measurement data is imported to HFSS and the tangential E field data is obtained from simulation.

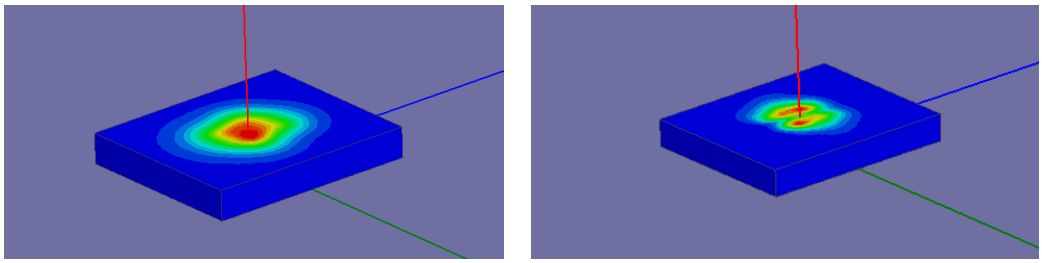

(a) (b)

Figure 3.22 Tangential E and H fields on Huygens's surface at 125MHz

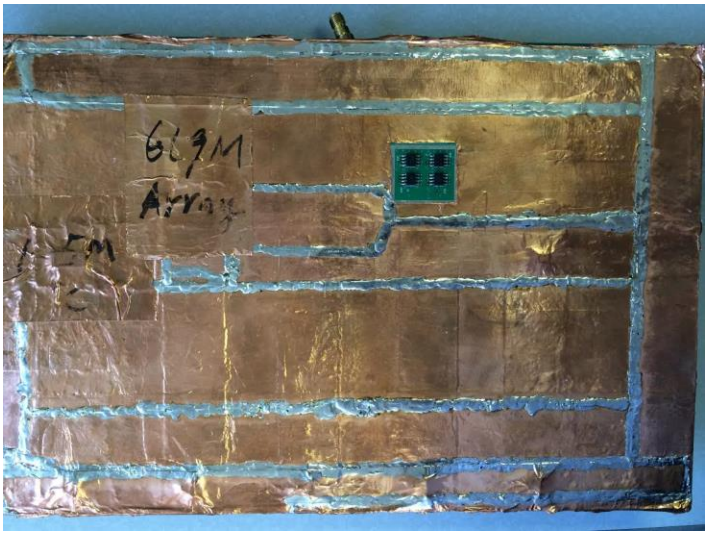

Figure 3.23 IC array on a large ground plane

With the same procedure as the U-shape trace source reconstruction, far-field is calculated based on Huygens's Principle and then matched with $\mathbf{J_z}$, $\mathbf{M_x}$ and $\mathbf{M_y}$ dipoles. Each of the dipole has one and placed at the center of the IC 1mm above it.

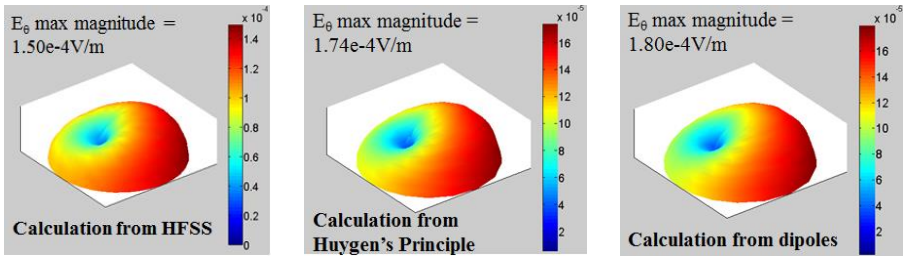

(a) (b) (c)

Figure 3.24 125MHz Far-field $\mathbf{E}_\theta$ comparison on 3m sphere between (a) HFSS simulation (b) Huygens's calculation (c) Equivalent dipole calculation

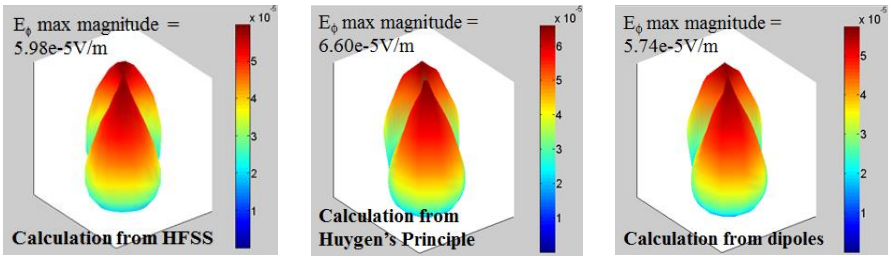

(a) (b) (c)

Figure 3.25 125MHz Far-field $\mathbf{E}_\phi$ comparison on 3m sphere between (a) HFSS simulation (b) Huygens's calculation (c) Equivalent dipole calculation

The far-field from Huygens'ss calculation and from equivalent dipoles match well. Then, the calculated dipoles for far-field construction are divided into dipole arrays. The value summation of the dipole array is same with the original calculated value. All 6 types of dipoles are distributed uniformally on an area of 8mm*8mm rectangular. The number of each type is 25.

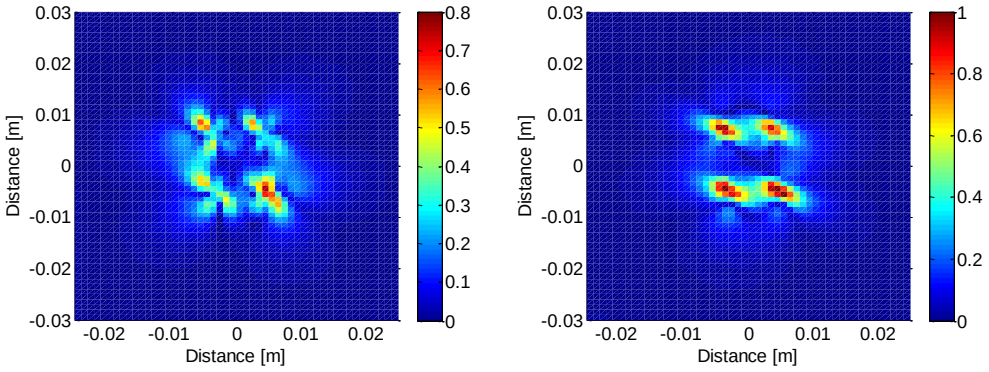

(a) (b)

Figure 3.26 125MHz Tangential H fields on top surface of Huygens's box from measurement (a) H_x (b) H_y

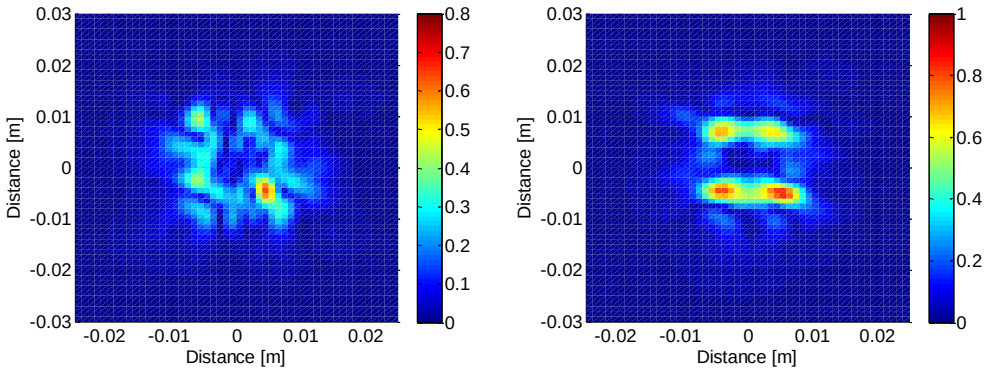

(a) (b)

Figure 3.27 125MHz Tangential H fields on top surface of Huygens's box from dipole reconstruction (a) H_x (b) H_y

The E and H fields on the top surface of the Huygens's box are compared with dipole calculation results. The results have resonable agreement.

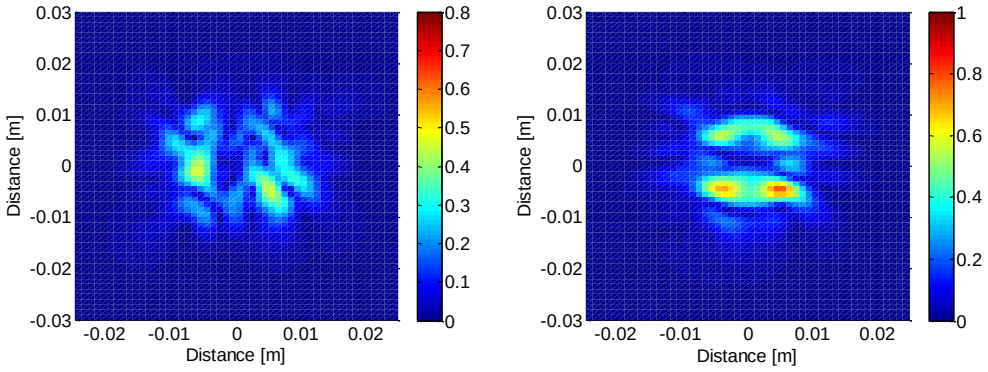

(a) (b)

Figure 3.28 125MHz Tangential H fields magnitude on top surface of the Huygens's box from dipole reconstruction (only $\mathbf{J_z}$, $\mathbf{M_x}$, and $\mathbf{M_y}$ dipoles are used) (a) H_x (b) H_y

With only $\mathbf{J_z}$, $\mathbf{M_x}$, and $\mathbf{M_y}$ dipoles used for matching near-field on the Huygens'ss surface, the magnitude of the reconstructed fields will have a big difference compared with the measured fields. All six types of dipoles are needed for a good prediction of near-field.

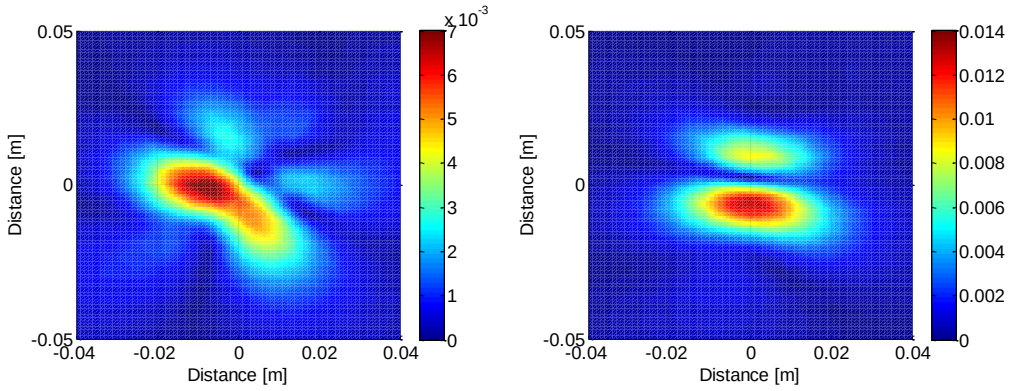

(a) (b)

Figure 3.29 125MHz tangential H fields magnitude (A/m) on 20mm plane from simulation (a) H_x (b) H_y

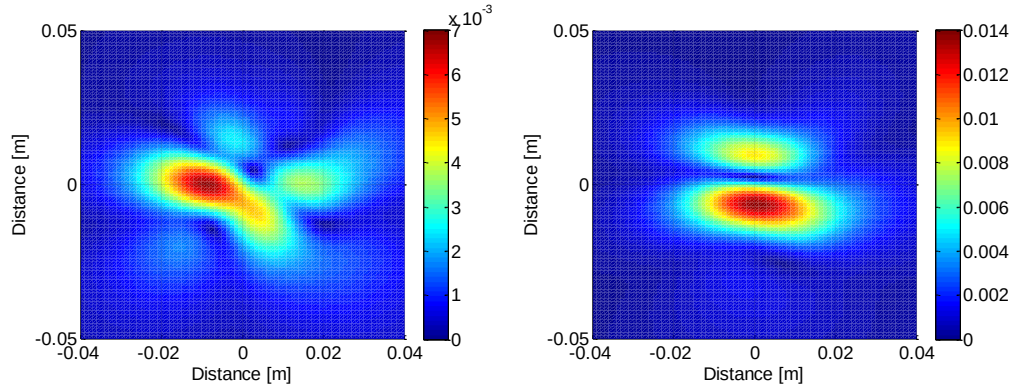

(a) (b)

Figure 3.30 125MHz tangential H fields magnitude (A/m) on 20mm plane from dipole reconstruction (a) H_x (b) H_y

The same IC is also tested at 1GHz and 2GHz. The far-field is firstly matched with $\mathbf{J_z}$, $\mathbf{M_x}$ and $\mathbf{M_y}$ dipoles. Then, near-field on the top Huygens's surface is matched

with $\mathbf{J_x}$, $\mathbf{J_y}$, $\mathbf{J_z}$, $\mathbf{M_x}$, $\mathbf{M_y}$ and $\mathbf{M_z}$ dipoles. The dipoles are all uniformly distributed on the area of the U-shape trace 1mm above it. Each type of dipole has a number of 25.

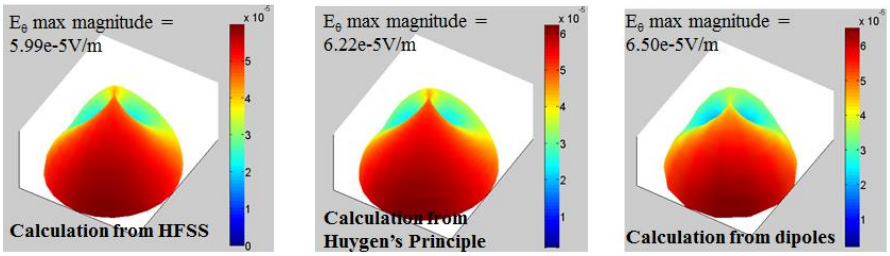

Figure 3.31 1GHz Far-field $\mathbf{E}_\theta$ comparison on 3m sphere between (a) HFSS simulation (b) Huygens's calculation (c) Equivalent dipole calculation

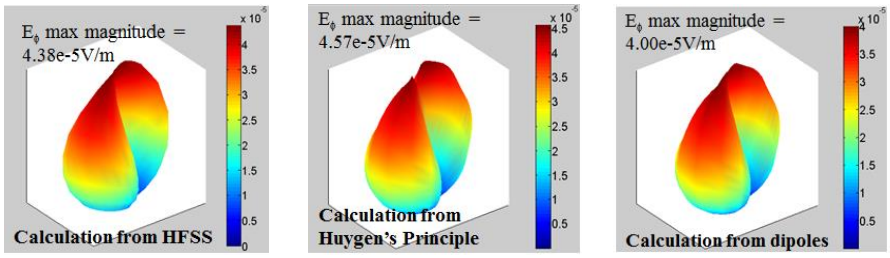

Figure 3.32 1GHz Far-field $\mathbf{E}_\phi$ comparison on 3m sphere between (a) HFSS simulation (b) Huygens's calculation (c) Equivalent dipole calculation

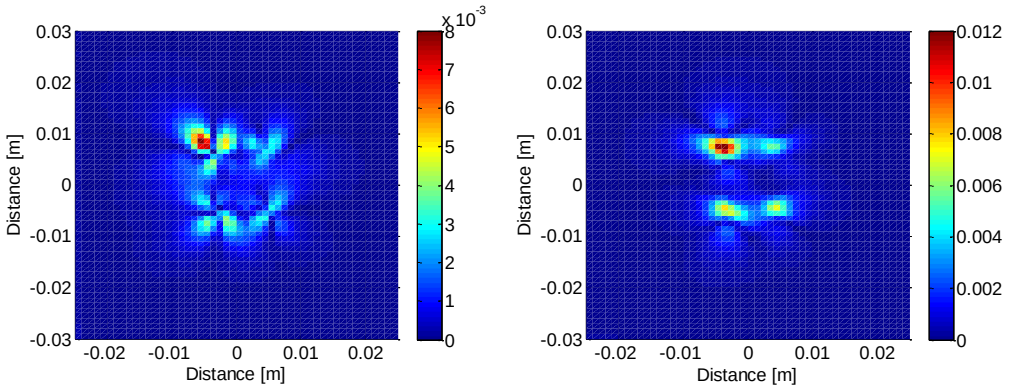

(a) (b)

Figure 3.33 1GHz Tangential H fields magnitude (A/m) on top surface of Huygens's box from measurement (a) H_x (b) H_y

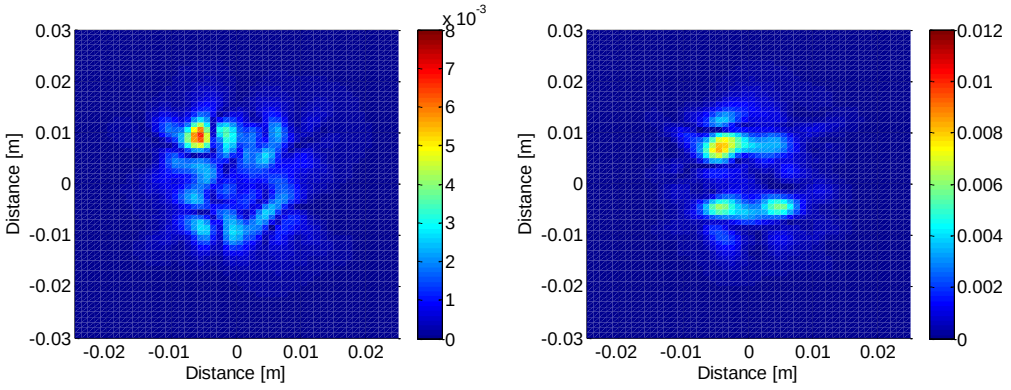

(a) (b)

Figure 3.34 1GHz Tangential H fields magnitude (A/m) on top surface of Huygens's box from dipole reconstruction (a) H_x (b) H_y

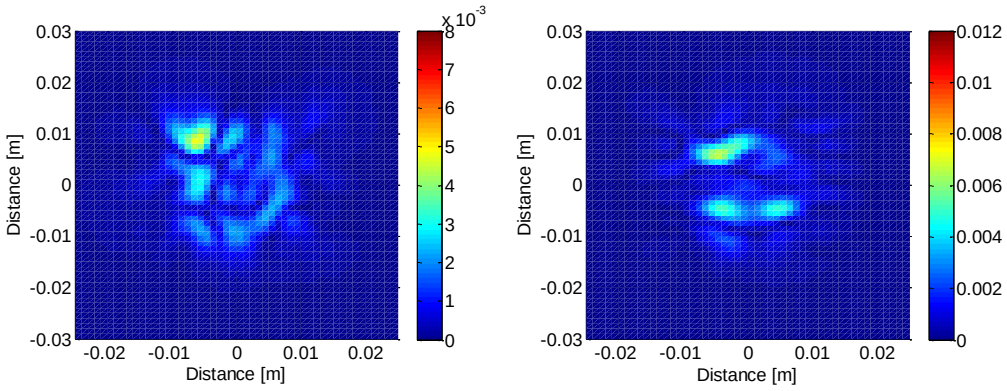

(a) (b)

Figure 3.35 1GHz Tangential H fields magnitude on top surface of the Huygens's box from dipole reconstruction (only $\mathbf{J_z}$, $\mathbf{M_x}$, and $\mathbf{M_y}$ dipoles are used) (a) H_x (b) H_y

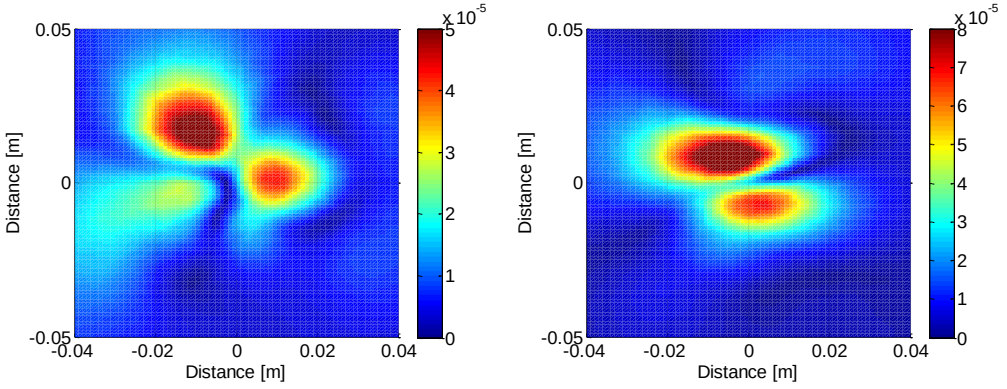

(a) (b)

Figure 3.36 1GHz tangential H fields magnitude (A/m) on 20mm plane from simulation (a) H_x (b) H_y

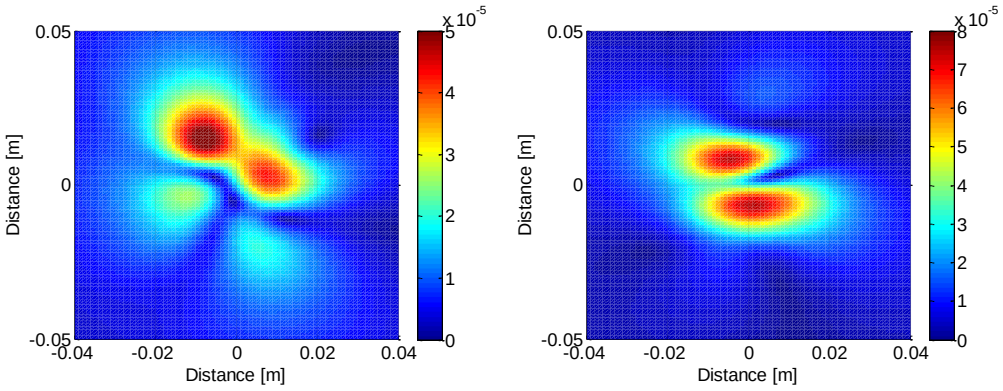

(a) (b)

Figure 3.37 1GHz tangential H fields magnitude (A/m) on 20mm plane from dipole reconstruction (a) H_x (b) H_y

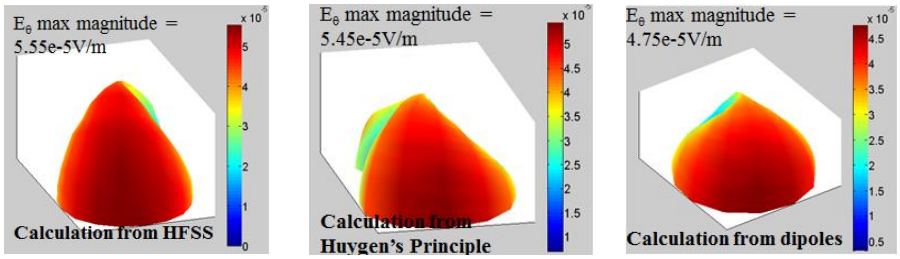

(a) (b) (c)

Figure 3.38 2GHz Far-field $\mathbf{E}_\theta$ comparison on 3m sphere between (a) HFSS simulation (b) Huygens's calculation (c) Equivalent dipole calculation

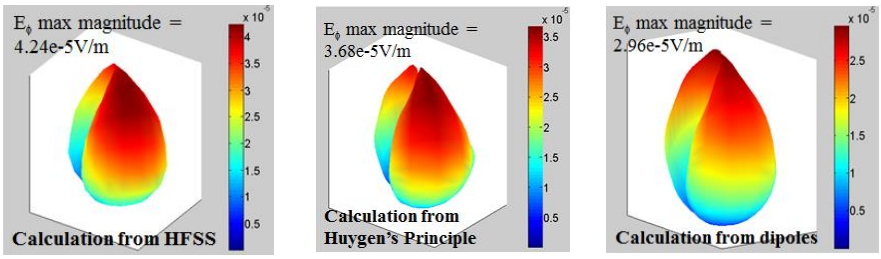

(a) (b) (c)

Figure 3.39 2GHz Far-field $\mathbf{E}_\phi$ comparison on 3m sphere between (a) HFSS simulation (b) Huygens's calculation (c) Equivalent dipole calculation

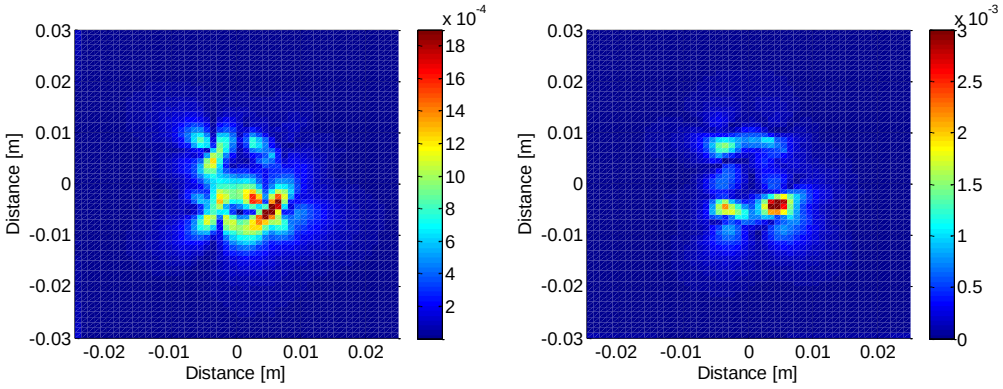

(a) (b)

Figure 3.40 2GHz Tangential H fields magnitude (A/m) on top surface of Huygens's box from measurement (a) H_x (b) H_y

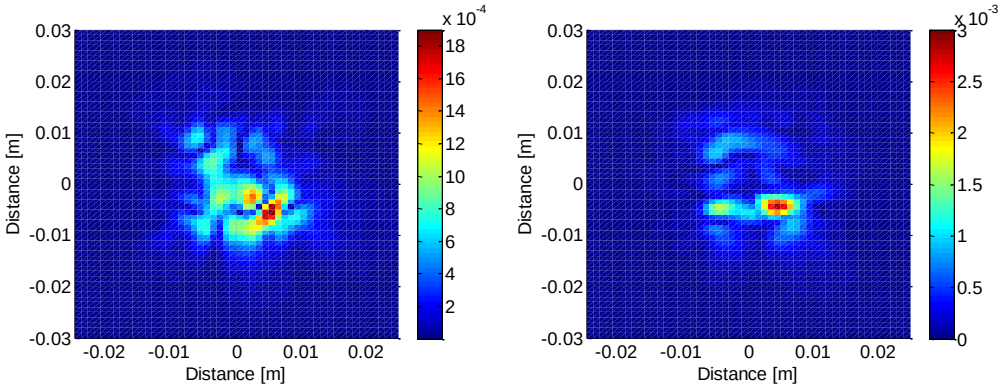

(a) (b)

Figure 3.41 2GHz Tangential H fields magnitude (A/m) on top surface of Huygens's box from dipole reconstruction (a) H_x (b) H_y

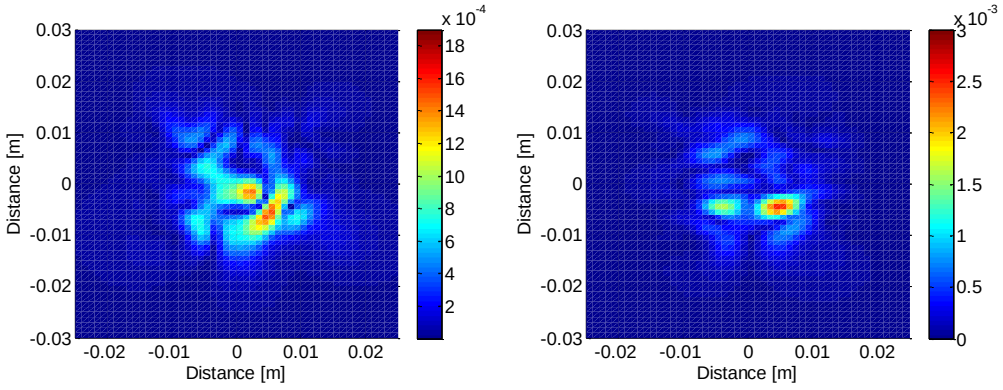

(a) (b)

Figure 3.42 2GHz Tangential H fields magnitude on top surface of the Huygens's box from dipole reconstruction (only $\mathbf{J_z}$, $\mathbf{M_x}$, and $\mathbf{M_y}$ dipoles are used) (a) H_x (b) H_y

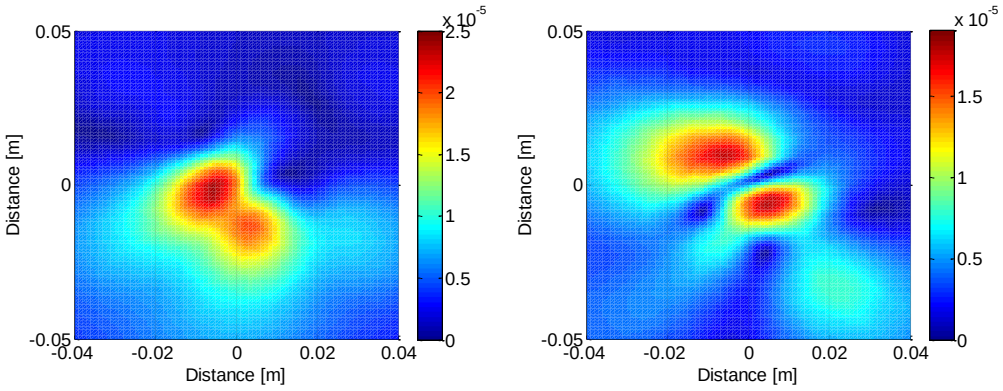

(a) (b)

Figure 3.43 2GHz tangential H fields magnitude (A/m) on 20mm plane from simulation (a) H_x (b) H_y

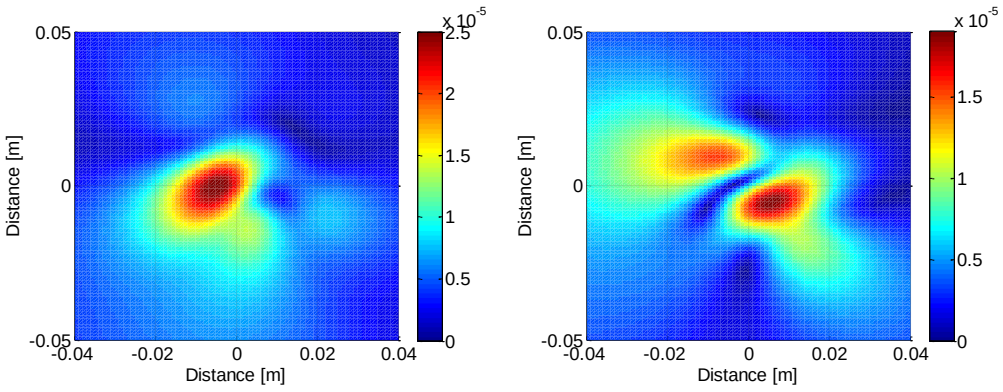

(a) (b)

Figure 3.44 2GHz tangential H fields magnitude (A/m) on 20mm plane from dipole reconstruction (a) H_x (b) H_y

Far-field at 3m is further validated by comparing with measurement results. The Ez component maximum magnitudes of far-field at 125MHz, 1GHz and 2GHz are compared with dipole reconstruction results.

Frequency	E_z maximum magnitude from measurement (dBuV/m)	E_z maximum magnitude from Huygen's principle calculation (dBuV/m)	E_z maximum magnitude from equivalent dipole calculation (dBuV/m)
125MHz	37	44.80	44.86
1GHz	35	33.18	35.88
2GHz	34	34.72	34.53

Figure 3.45 $\mathbf{E_z}$ magnitude maximum value comparison between measurement results and dipole reconstruction results

The far-field $\mathbf{E_z}$ magnitude maximum value from equivalent dipole calculation and from Huygens's Principle has reasonable correlation at frequencies tested.

4. CONCLUSIONS

A new equivalent dipole moment model is proposed in the paper for reconstructing the radiation source of an IC above a large ground plane. The equivalent dipoles are obtained through the near-field scanning techniques. Tangential electric and magnetic fields on the Huygens's surface enclosing the DUT are obtained through simulation or near-field measurement. The far-field is obtained from measurement or calculation from known near-field on the Huygens's surface with the Huygens's Principle. The two-step method is established which is to fit far-field with a set of dipoles first and then add in another set of dipoles to correct the near-field. In the near-field fitting process, the dipoles obtained for far-field fitting are further divided into a dipole array for more accurate of near-field matching. This set of dipoles is capable of predicting both near- and far-field radiation from an IC. Two examples are used to validate the method. A U-shape trace model is built in HFSS simulation and the equivalent dipole model is verified by simulation. An IC array near- and far-field radiation is measured and equivalent dipole-moment model is obtained and verified at 125MHz, 1GHz and 2GHz. The number of dipole needed in this new method is small compared with early studies which provides an easy and fast way for implementation of system-level simulation.

BIBLIOGRAPHY

[1] Xin Tong, David W.P. Thomas, Angela Nothofer, Phillip Sewell, and Christos Christopoulos, "Modeling Electromagnetic Emissions From Printed Circuit Boards in Closed Environments Using Equivalent Dipoles," *Electromagnetic Compatibility, IEEE Transactions,* vol.52, no.2, pp.462,470, May 2010.

[2] H. Weng, D.G. Beetner, and R.E. DuBroff, "Prediction of Radiated Emissions Using Near-Field Measurements," *Electromagnetic Compatibility, IEEE Transactions,* vol.53, no.4, pp.891,899, Nov. 2011

[3] J. Shi, M.A. Cracraft, J. Zhang, R.E. DuBroff, and K. Slattery, "Using near-field scanning to predict radiated fields," *Electromagnetic Compatibility, 2004. EMC 2004. 2004 InternationalSymposium*, vol.1, no., pp.14,18 vol.1, 9-13 Aug. 2004

[4] Alvarez, Y.; Rodríguez, M.; Las-Heras, F.; Hernando, M.M., "On the Use of the Source Reconstruction Method for Estimating Radiated EMI in Electronic Circuits," *Instrumentation and Measurement, IEEE Transactions*, vol.59, no.12, pp.3174,3183, Dec. 2010.

[5] M. Hernando, A. Fernandez, M. Arias, M. Rodriguez, Y. Alvarez, and F. Las-Heras, "EMI radiated noise measurement system using the source reconstruction technique," *IEEE Trans. Ind. Electron.*, vol. 55, no. 9, pp. 3258–3265, Sep. 2008.

[6] Y. Vives, C. Arcambal, A. Louis, F. de Daran, P. Eudeline, and B. Mazari, "Modeling magnetic radiations of electronic circuits using near-field scanning method," *IEEE Trans. Electromagn. Compat.*, vol. 49, no. 2, pp. 391– 400, May 2007

[7] D. Baudry, C. Arcambal, A. Louis, B. Mazari, and P. Eudeline, "Applications of the near-field techniques in EMC investigations," *IEEE Trans. Electromagn. Compat.*, vol. 49, no. 4, pp. 805–815, Nov. 2007.

[8] Vives-Gilabert, Y., Arcambal, C., Louis, A., de Daran, F., Eudeline, P., and Mazari, B., "Modeling Magnetic Radiations of Electronic Circuits Using Near-Field Scanning Method," *Electromagnetic Compatibility, IEEE Transactions*, vol.49, no.2, pp.391,400, May 2007.

[9] X. Ren, P. Maheshwari, Y. Zhang, V. Khilkevich, J. Fan, Y. Zhou, Y. Bai and X. Yu, "The impact of near-field scanning size on the accuracy of far-field estimation," *Electromagnetic Compatibility (EMC), 2014 IEEE International Symposium*, vol., no., pp.582,587, 4-8 Aug. 2014

[10] Z. Yu, J.A. Mix, S. Sajuyigbe, K.P. Slattery, and J. Fan, "An Improved Dipole-Moment Model Based on Near-Field Scanning for Characterizing Near-Field Coupling and Far-Field Radiation From an IC," *Electromagnetic Compatibility, IEEE Transactions*, vol.55, no.1, pp.97,108, Feb. 2013

[11] C. A. Balanis, "*Antenna Theory, Analysis and Design*" New York: Harper & Row, 1982.

VITA

Xiao Ren was born in Shanxi, China. In July 2012, she obtained a bachelor's degree in College of Electrical Engineering from Chongqing University, Chongqing, R.P. China.

In August 2012, she enrolled at Missouri University of Science and Technology to pursue a master's degree of Electrical and Computer Engineering under the guidance of Dr. Jun Fan and Dr. Yaojiang Zhang. Her research interest is near-field scanning techniques for RFI problems. In August, 2015, she received her MS in Electrical Engineering from Missouri University of Science and Technology.